Mid-infrared spectroscopy of starbursts : from Spitzer-IRS to JWST-MIRI

Martínez-Galarza, J.F.

CHAPTER 4

Outlook: Recent star formation in nuclear starbursts[1]

In this outlook chapter we carry out a pilot study on the modelling of spectral energy distributions (SEDs) of unresolved starbursts in the Local Universe. We apply our Bayesian SED fitting tool to the MIR spectra of a small sample of starbursts galaxies, in order to investigate differences in their physical properties and recent star formation histories (SFHs). Our robust method finds significant differences in the recent SFHs of the studied objects. For example, we find that in our small sample of targets, the most massive, recently formed clusters were born in regions with comparatively less intense SFRs, where the molecular gas is depleted. Moreover, we find that these gas-poor systems show the largest contribution from very recent (< 1 Myr) massive star formation, which might be indicative of positive feedback from the inferred massive clusters, at the end of a more quiescent period of star formation in these systems. Our pilot study is encouraging, although the small size of the sample does not yet allow for the formulation of general trends. We thus propose a systematic study of a large sample of starburst SEDs, using the present method, to corroborate our findings.

[1] J.R. Martínez-Galarza, B. Groves, B. Brandl, in preparation.

4.1 Introduction

A considerable number of nearby galaxies show increased rates of star formation per unit of stellar mass, as compared to the Milky Way. Their bolometric luminosities are dominated by the UV radiation field of young massive stars formed within the last 10: Myr, the product of a fast gas depletion process. These *starbursts* (Weedman et al. 1981) are often related to galactic mergers, but their nature and triggering mechanism has not been fully established. Since massive star formation occurs in regions heavily enshrouded by dust, starburst have very high infrared luminosities, the product of the processing of stellar UV light by dust particles in the interstellar medium (ISM). The incidence of these star formation-powered, very luminous galaxies increases with cosmic distance and at redshifts beyond $z \sim 1$, the most luminous members of this class account for most of the cosmic star formation rate (SFR) density (Elbaz & Cesarsky 2003). Furthermore, infrared emission from dust accounts for about half of the bolometric luminosity of the Universe (Dole et al. 2006). Thus, the study of the infrared properties of starbursts, both near and far, and its relation to their internal physics, is crucial in the understanding of massive star formation throughout cosmic history.

Fitting the observed integrated SEDs of starbursts using predictions from theoretical models is an elegant way to relate measured observables to the internal physics of these systems. A systematic application of a reliable fitting method to a selection of starburst galaxies can provide clear answers to the questions of what triggers starbursts and how they relate to the internal physics and local conditions of the ISM. This information is instrumental on the interpretations of distant systems for which only unresolved information is available. The MIR portion of the starburst SEDs is of particular relevance for several reasons. First, for distant, obscured objects only data at mid-infrared and far-infrared wavelengths are available. Also, the effects of extinction are much less significant at infrared wavelengths and allow a more accurate determination of SFRs, in contrast with ultraviolet (UV) determination methods, which require extinction corrections of a factor of ~ 10, as pointed out in Sargsyan & Weedman (2009). The same authors have shown that infrared discovered starbursts are not dustier than starbursts discovered using other wavelength regimes, thus minimizing selection effects.

SED fitting has another advantage over monochromatic SFR diagnostics: it does not only quantify recent star formation in galaxies, but it also constrains the plausible values of other physical parameters involved in the process of star formation. While monochromatic, MIR diagnostics have been successful in measuring the SFRs in galaxies (Calzetti et al. 2005, Relaño et al. 2007, Alonso-Herrero et al. 2006, Rieke et al. 2009), they have provided little insight into the reasons for the enhanced star formation in starbursts. However, SED fitting should be applied with care, because of the many degeneracies that arise both from observational errors and intrinsic inter-dependencies of the model parameters. Also, a successful method should use as much information as possible from the integrated SEDs, including the nebular line fluxes that are instrumental in the determination of physical conditions such as ionization state of the gas and the ISM pressure. So far, a statistically robust method for fitting the SEDs of galaxies, including both thermal continuum and nebular lines, has been lacking.

In this outlook chapter we investigate the physics of star formation in a small selection of starburst galaxies from Brandl et al. (2006) (B06 hereafter), with different morphologies and infrared luminosities. For this purpose we apply the fitting tool presented in Chapter 2 to the MIR spectra of the nuclear regions of these galaxies to obtain robust constraints of the SFRs, compactness, ISM pressure, and amount of currently ongoing massive star formation in these galaxies, in a similar way as we did for the NGC 604 star forming region in Chapter 3. In §4.2 we present the basic parameters of the selected galaxies and discuss their morphologies. We continue with a description of their mid-infrared spectra and the results of the fitting process in §4.3. In §4.4 we discuss our results and show our main findings in terms of the differences in the recent SFHs of the starbursts in the sample. We summarize our results in §4.5.

4.2 Sample of galaxies

4.2.1 Selection criteria

The sample of starburst galaxies presented in B06 includes both "pure" starbursts as well as objects with a weak contribution to the dust heating from active galactic nuclei. They also cover a broad range of metallicities, from sub-solar to supra-solar metallicities. Additionally, while most of them show evidence of mergers or some type of interaction with near companions, at MIR wavelengths some of them appear as single nuclei, while others clearly show the presence of more than one nucleus, and one of them appears as a circumnuclear star-forming ring. For the present study, we have selected a sub-sample of this group of starbursts, composed of five objects that comply with two selection criteria: *(a)* the contribution from an AGN to the luminosity of the nucleus is nonexistent or marginal, and *(b)* their metallicities are close to the solar value ($0.8Z_{\odot} \leq Z \leq 1.4Z_{\odot}$). The second criterion helps us reduce the parameter space investigated with our models and allows us to focus on specific parameters such as compactness, ISM pressure, and amount of embedded star formation.

The variations of MIR spectral properties with metallicity have been studied by several authors, both from observations and theory. For example, in a study of the SINGS sample of galaxies (Kennicutt et al. 2003), Draine et al. (2007) have measured the PAH index $q_{\rm PAH}$ (the percentage of dust mass contributed by PAHs) as a function metallicity, and found a bi-modal distribution of the $q_{\rm PAHS}$ values, with $q_{\rm PAH} \sim 1\%$ for galaxies $12 + \log_{10}({\rm O/H_{gas}}) < 8.1$, and $q_{\rm PAH} \sim 3.5\%$ for galaxies $12 + \log_{10}({\rm O/H_{gas}}) > 8.1$. This reflects in stronger PAH features in metal-rich galaxies. From the point of view of physical modelling, we expect metallicity to affect the MIR spectra of starbursts in several ways (Groves et al. 2008). First, there is an intrinsic change in the stellar radiation field with metallicity. Also, different metal abundances result in variations in the temperature and line emission from ionized regions, and of course, there is also a change in the grain composition with metallicity, which results in different effective dust temperatures and a resulting change in the MIR and FIR thermal continuum.

By selection, none of the galaxies has an AGN contribution to their internal energy.

Although B06 do not find a systematic difference between "pure" starbursts and galaxies with a weak contribution from AGNs for most of their galaxies, some differences are expected. The high energy photons and strong radiation field related to dust and gas heating by an active nucleus prevent the formation of PAH molecules or destroy them rapidly, and hence these features tend to be weak in AGN dominated galaxies. Also, the spectral slope can be used as a discriminator between starbursts and AGN activity, as first noticed using IRAS data (e.g. Wang 1992). In the following subsections we briefly describe some general properties of our sample galaxies.

4.2.2 Basic properties

In Table 4.1 we list the basic properties of the galaxies studied here. We want to emphasize the fact that, even though they all have similar infrared luminosities, they are different in many other aspects, such as their molecular gas content (the fuel for star formation), surface brightness, and galactic host morphology. They are also located at a broad range of distances, which directly affects their surface brightness and also the fraction of the total flux that falls within the *Spitzer*-IRS spectrometer slit in the B06 study. This also means that not in all cases the measured spectra corresponds to the nuclear region only. For the more distant objects, the larger structure of the host galaxy fits within the spectrometer slit. The selected galaxies are shown in Fig. 4.1 as they appear at mid-IR wavelengths

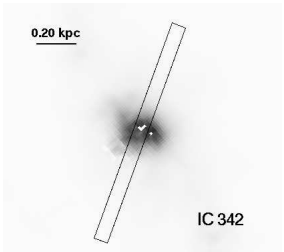

(a) IC 342

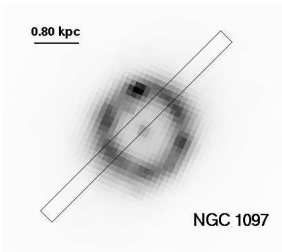

(b) NGC 1097

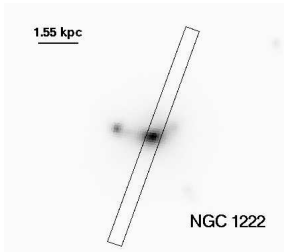

(c) NGC 1222

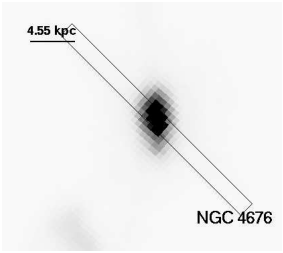

(d) NGC 4676

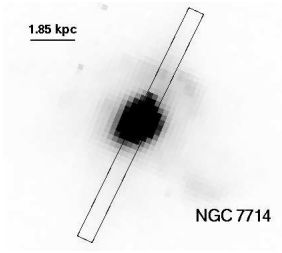

(e) NGC 7714

Figure 4.1 IRAC 8 μm images of our selected galaxies, with the IRS short-low slit overimposed for comparison.

Table 4.1 Properties of sample galaxies.

Name	α	δ	D[a] [Mpc]	$\log(L_{\rm IR})$[a] [$L_\odot$]	Z[b] [$Z_\odot$]	$M_{\rm mol}$[c] [$M_\odot$]	SFR[d] [$M_\odot$ yr^{-1}]	$\log(M_*)$[e] [$M_\odot$]
IC 342	3 46 48.51	+68 05 46.0	4.6	10.17	0.80	1.0×10^7	1.87	7.0
NGC 1097	2 46 19.08	-30 16 28.0	16.8	10.71	1.38	1.3×10^9	5.0	9.0
NGC 1222	3 08 56.74	-02 57 18.5	32.3	10.60	1.07	$< 10^8$	6.8	5.1
NGC 4676	12 46 10.10	+30 43 55.0	94.0	10.88	1.17	5.0×10^9	15.8	~ 7.0
NGC 7714	23 36 14.10	+02 09 18.6	38.2	10.72	1.17	$< 10^8$	6.0	6.9

[a] Distances and IR luminosities taken from B06.

[b] Metallicities are taken from Lebouteiller et al. (2011), except for IC 342 and NGC 1097, whose metallicities have been taken from Crosthwaite et al. (2001), and Dors et al. (2008), respectively.

[c] Molecular gas masses taken from Israel & Baas (2003), Gerin et al. (1988), Chini et al. (1992), Yun & Hibbard (2001) and Smith & Struck (2001), respectively.

[d] Star formation rates taken from the KINGFISH website, Hummel et al. (1987), Brandl et al. (2006), Mineo (2011) and Gonzalez-Delgado et al. (1995).

[e] Stellar masses taken from Schinnerer et al. (2008), Quillen et al. (1995),(Beck et al. 2007), de Grijs et al. (2003), and González Delgado et al. (1999).

4.2.3 Morphologies

Although they are all classified as nuclear starbursts, the galaxies in our sample have a variety of morphologies and luminosities. For most of the galaxies, the morphology is due to ongoing or recent mergers or galactic collisions. The star-forming ring in the nucleus of NGC 1097 is clearly resolved at 8 μm while in the other galaxies the IR emission is more compact. The scaling of the orders has been performed accordingly, as described in B06. Here we are interested in studying if there is a clear relation between the nucleus morphology, the measured spectra, and the underlying physics of star formation.

4.2.4 Measurements from the literature

IC 342

The face-on late-type barred spiral IC 342 belongs to the Maffei Group of galaxies and harbors a nuclear starburst powered by the infall of molecular gas via the spiral bar. The inner 400 pc of IC 342 have roughly the same infrared luminosity and stellar mass as the inner 400 pc of the Milky Way (Lebrón et al. 2011). Early CO and [C I] measurements showed that the molecular gas is strongly concentrated in the nucleus of this galaxy, with surface gas densities of $\sim 70\,M_\odot\,pc^{-2}$ (Israel & Baas 2003). These authors also report that at least half of the molecular gas is associated with hot photon-dominated regions (PDR) in the nuclear region. Negative feedback from the nuclear starburst on the star formation has been reported in Schinnerer et al. (2008), who claim that the efficiency of gas inflow towards the nucleus via the bar is reduced by the effect of stellar winds and supernovae. This is in agreement with the recent detection of depleted very dense gas near the sites of recent star formation (Meier et al. 2011), which indicate a high star formation efficiency. Using X-ray data, Mak et al. (2011) have recently detected supernova remnant activity near the nuclear starburst.

NGC 1097

NGC 1097 is a barred spiral galaxy with a weak active nucleus (Phillips et al. 1984). It has been known for several decades now that there is a star-forming ring-like structure with a diameter of $\sim$ 1 kpc that surrounds the nuclear region. This ring is rich in molecular gas, and has a sub-structure of azimuthal, very compact clumps that are bright at infrared wavelengths, with estimated masses of the order of $10^7\,M_\odot$ (Walsh et al. 1986). Models of the star formation activity in the ring indicate that it is better explained by an instantaneous burst of star formation that occurred 6-7 Myr ago (Kotilainen et al. 2000). Recent star formation has also been detected at very small distances (< 10 pc) from the active nucleus (Storchi-Bergmann et al. 2005), but evidence has been gathered that even in this very central region star formation, rather than the central engine, is responsible for the dust heating (Mason et al. 2007). More recently, Herschel observations have shown that more than 60% of the FIR thermal emission from dust in NGC 1097 comes from the central

ring (Sandstrom et al. 2010), which has a total molecular mass of $\sim 1.3\times10^9\,M_\odot$ (Gerin et al. 1988). FIR cooling lines are indicative of ionized gas densities between 150-400 cm^{-3}, and a strong radiation field near the ring clumps (Beirão et al. 2010). Although such star-forming rings are common to many galaxies, it is not yet clear what the triggering mechanism is for such structures.

NGC 1222

NGC 1222 is a spheroidal galaxy with a nuclear starburst whose SFR is about 4 times that of the host galaxy (Petrosian & Burenkov 1993). This object has been recognized as a peculiar galaxy due to its bright MIR nebular emission lines and spectral properties, that resemble those of a dwarf metal-poor galaxy. In fact, NGC 1222 has the highest deduced upper limit for the stellar mass in solar-metallicity galaxies, between 40 $M_\odot$ and 100 $M_\odot$ (Beck et al. 2007). Another peculiarity has to do with its low content of molecular mass, for which only upper limits have been detected (Elfhag et al. 1996). Beck et al. (2007) also speculate that the peculiarities of this galaxy are due to a double merger with two nearby companions. The ionization state of the gas in the nuclear region is compatible with a stellar population containing 1.4×10^5 O stars, that are contained within a region of size < 500 pc. The starburst is characterized by a high ISM gas density ($\log n = 4.1$ cm^{-3}), compared to other starbursts, as determined using FIR emission lines (Malhotra et al. 2001).

NGC 4676

This interacting pair of galaxies has been popularly known as "the Mice", and it is classified as an early stage merger in the Toomre sequence (Toomre 1977). Here we analyze the spectrum of the northern galaxy (NGC 4676A), which contains most of the PAH and CO emission in the system. In fact, NGC 4676A shows a peculiar variation of the PAH feature ratios, with a $PAH_{7.7\mu m}/PAH_{11.3\mu m}$ decreasing toward the nucleus, indicating a deficit of ionized PAHs in the center with respect to neutral PAHs (Haan et al. 2011). This is even more surprising given the fact that no weak active nucleus has been identified in the central region of this galaxy. Using NIR spectroscopy, Chien et al. (2007) find evidence for a young (< 6 Myr) stellar population in the nucleus of this northern galaxy, which is indicative of a recent starburst. This is in agreement with starburst-driven galactic winds outflowing along the minor axis of the galaxy, as revealed by *Chandra* X-ray observations (Read 2003). The nuclear region is characterized by a compact ($R < 2$ kpc) molecular complex that contains $\sim 20\%$ of the total molecular mass, which is estimated to be $M_{H2} \sim 5\times10^9\,M_\odot$ and have a density of $N_{H2} \sim 6\times10^{22}$ cm^{-2} in the central region (Yun & Hibbard 2001).

NGC 7714

This peculiar spiral was the first galaxy to be designated as a *starburst* (Weedman et al. 1981), and has since become a prototype for these systems. It has a nearby interacting

post-starburst companion (NGC 7715) with which it had a close, off-center encounter between 100 and 200 Myr ago (Struck & Smith 2003). Its star formation activity is heavily concentrated in the nucleus, though it also shows star-forming regions across the deformed galactic disk. The strong nuclear Hα emission, bright PAH features and weak silicate absorption features (Gonzalez-Delgado et al. 1995, Brandl et al. 2004) suggest that the nuclear activity is powered by an unobscured starburst with a total mass of $\sim 10^7$ $M_\odot$, while the weak [Fe II] emission (Matsuoka et al. 2011) and strong star formation-triggered bipolar winds traced by X-ray observations (Taniguchi et al. 1988) seem to rule out the presence of an AGN in the nucleus of the galaxy. Like NGC 1222, this galaxy also shows strong forbidden lines, compatible with a population of $\sim 2 \times 10^4$ O stars (Smith et al. 1997). Modelling of the UV spectrum gives an age of 5 Myr for the nuclear starburst (González Delgado et al. 1999), but evidence for an older population (15-50 Myr) in the same region has also been found (Lançon et al. 2001). Taniguchi et al. (1988) estimate a total mass of ionized gas of 1.9×10^6 $M_\odot$.

4.3 Results

4.3.1 MIR spectra of the selected galaxies

Fig. 4.2 shows the IRS spectra of our sample galaxies. A comprehensive description and analysis of the spectral features, including PAH emission, nebular lines and thermal continuum can be found in B06. Of relevance here is the fact that not all the wavelength range shown in the figure is covered by a single order (and hence by a single slit) of the spectrometer, and hence a scaling factor is necessary to match the orders together. As discussed in the B06, the IRS short-low (SL) fluxes were scaled up to match the IRS long-low (LL) slit fluxes, which are measured with a larger slit (only the small SL slit is shown in Fig. 4.1). The motivation for this choice, in the case of the nuclear starbursts discussed here, is that the mismatch is due to some nuclear flux missed by the SL slit, and not to unrelated extended flux. Hence, scaling the SL fluxes up accounts for this missing nuclear flux, and the resulting spectra represent the true integrated starburst flux. We will discuss this further in §4.4

The selected galaxies sample a fair range of spectral shapes. The most remarkable differences have to do with the relative strength of the PAH features with respect to the thermal continuum, the depth of the 9.7 μm silicate absorption feature and the intensity of the nebular lines. NGC 4676 has by far the strongest PAH emission and also the deepest silicate absorption, in contrast with NGC 7714, which has relatively weak PAHs and very little silicate absorption. These two objects only seem to represent the extremes between a heavily obscured and an unobscured starburst, although they are both the product of an interaction and have a similar age (5-6 Myr). The ionization of higher atomic states in the gas, as traced by the strength of the [Ne III]15.5μm and [S IV]10.5μm nebular line emission, is high in NGC 1222 and undetected in IC 342 and NGC 1097. The slope of the dust thermal continuum, measured in B06 using the $F_{15\mu\mathrm{m}}/F_{30\mu\mathrm{m}}$ ratio, is steeper for NGC 4676, and decreases in the following order: NGC 7714, NGC 1222, IC 342 and

NGC 1097.

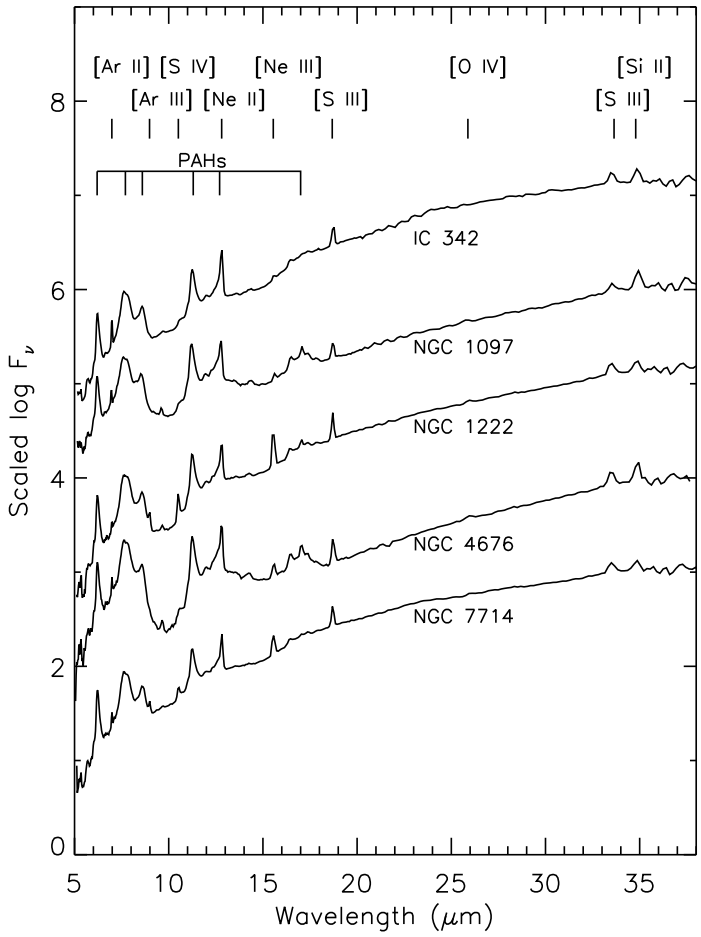

Figure 4.2 Mid-infrared spectra of our selected galaxies. All spectra are normalized to the flux at 30 μm and shifted one decade in logarithmic flux for comparison. The main spectral features are labelled.

4.3.2 Bayesian fitting of the spectra

General remarks

In order to investigate if there are fundamental differences in the physics of the interstellar medium between the galaxies in our sample, we applied the Bayesian fitting tool described in Chapters 2 and 3 to the spectra shown in Fig. 4.2. The tool provides a fit to the spectra, and robust constraints for the physical parameters on the models. We have used the age-averaged version of the galactic SEDs, which assumes a constant SFH over the last 10 Myr, as described in §2.5.4 of this thesis. Our assumption of a constant star formation history rather than an instantaneous burst of star formation is supported by several facts. First, while the SFR of the systems studied here are dominated by recent starbursts, there is also evidence for an age spread in the systems, as we have seen in §4.2. Rather than one or a few instantaneous star formation bursts, a continuous enhanced SFR over the last million years seems a more physical explanation for the age spread. Second, since the fixed size of the IRS slit translates into different physical scales at the distances of the galaxies, we cannot guarantee that, although dominating, the emission from the nuclear region is the only component of the spectra. Finally, we have seen in Chapter 2 that not even a single Giant H II Region such as 30 Doradus can be modelled assuming a single instantaneous burst, and hence a time-averaged approach seems more reasonable for distant counterparts of 30 Doradus.

The physical parameters studied here are the SFR, the compactness (C), the fraction of the total luminosity emitted in PDR regions ($f_{\rm PDR}$), the ISM ambient pressure (P_0/k) and the mass contribution of young, embedded objects ($f_{\rm emb}$), that accounts for very recent star formation in the systems. Additionally, it is possible to account for variations in the extinction, which at MIR wavelengths affects the depth of the 9.7 μm silicate absorption feature. We have described these parameters in §2.3.3. Here we will only remind the reader that in the age-averaged models used in the present chapter, these parameters represent the physical conditions in individual H II regions within the starbursts, averaged over the last 10 Myr. We have seen in Chapters 2 and 3 that these parameters are well constrained, and their derived values and uncertainties are robust. More importantly, we have shown that their values are related to the evolutionary stage of the H II regions, and hence they provide information on the physics that regulate the star formation in starbursts. By relating the derived parameters to the morphology and observables of these systems, we will learn about the local conditions in individual H II regions and the overall star formation characteristics of the starbursts.

Far-infrared photometry has been obtained for some of the galaxies in our sample using the Photodetector Array Camera and Spectrometer (PACS) instrument onboard the *Herschel Space Observatory*, but it is unfortunately not yet publicly available. Nevertheless, as we have seen in §3.4.2, while the *Herschel* data provides better constrains to the parameters, the best-fit estimates obtained with our tool remain unchanged when far-infrared data are included.

Name	$\log C$	$f_{\rm PDR}$	$f_{\rm emb}$	**SFR** $M_\odot\ {\rm yr}^{-1}$	$\log P_0/k$ K cm^{-3}
IC 342	$6.5^{+0.0}_{-0.5}$	> 0.80	$0.94^{+0.17}_{-0.38}$	$0.74^{+0.17}_{-0.03}$	> 7.0
NGC 1097	$5.0^{+0.5}_{-0.5}$	> 0.90	$0.25^{+0.19}_{-0.08}$	$5.18^{+0.77}_{-0.47}$	> 7.5
NGC 1222	$6.0^{+0.5}_{-0.5}$	> 0.80	$1.40^{+0.17}_{-0.53}$	$4.65^{+1.66}_{-0.38}$	> 5.0
NGC 4676	$5.0^{+0.5}_{-0.5}$	> 0.90	< 0.20	$21.23^{+3.89}_{-1.28}$	> 7.5
NGC 7714	$6.0^{+0.5}_{-0.5}$	> 0.75	$1.76^{+0.89}_{-0.44}$	$7.38^{+2.62}_{-0.62}$	> 6.5

Table 4.2 Best fit values for the model parameters in the galaxy sample. The uncertainties as derived from the Probability Distribution Functions (PDFs) are indicated.

Best fit parameters and uncertainties

In Fig. 4.3 we show the best fit models after applying the Bayesian tool to the spectra shown in Fig. 4.2, and in Table 4.2 we list the best fit parameters and their derived uncertainties.

The uncertainties are obtained from the 1-σ contours of the derived posterior probability distribution functions (PDFs), in the same fashion as they were derived in Chapters 2 and 3. The best fits shown in the figure emphasize the variation in the contributions from different components to the integrated spectra of our sample galaxies. In particular, the contribution from hot dust arising near the embedded objects, modelled here as Ultra Compact H II Regions (dotted blue line in the figure) varies considerably from galaxy to galaxy. The galaxy spectra are dominated by the PDR component, over the pure H II component, that contributes very little in all cases, although the uncertainties are larger for IC 342 and NGC 7714. The derived SFRs range from a Milky Way value for IC 342 up to 20 times the galactic value in NGC 4676, the northern galaxy of the Mice. For the ISM thermal pressure we can only establish lower limits, since the mid-IR spectrum is not very sensitive to this parameter. Only the nebular lines constrain P_0/k, which falls near the high pressure end for most of our galaxies, those with the lowest limits being NGC 1222 and NGC 7714.

An interesting fact is that galaxies with weak PAH emission, such as NGC 1222 and NGC 7714 do not necessarily imply a small contribution from PDR regions. In fact, as we have noticed, all galactic spectra are dominated by a PDR-like component and the best fit model gives $f_{\rm PDR}$ close to unity for all but one of the galaxies. An increase in the level of the MIR thermal continuum, for example by adding the embedded component, can result in a relatively weaker PAH emission. However, the derived uncertainties do show that the lower limits to the PAH contribution tend to be smaller for galaxies that show weak PAH emission.

Another important difference has to do with the depth of the 9.7 μm silicate absorption feature, which is a measure of the extinction towards these galaxies. As we have mentioned, this can be related to the inclination at which we observe the galaxy, or simply to

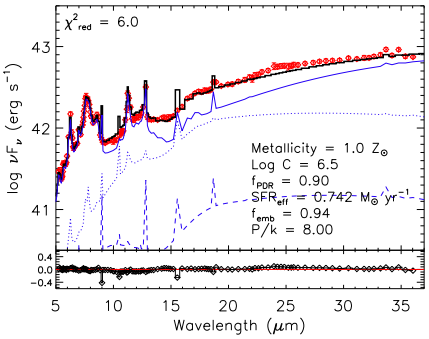

(a) IC 342

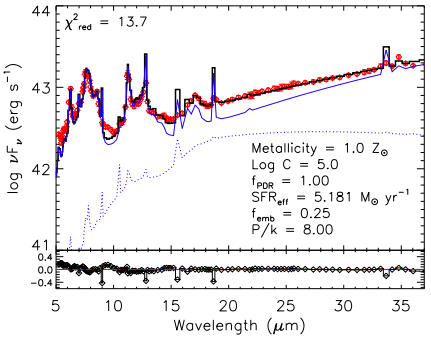

(b) NGC 1097

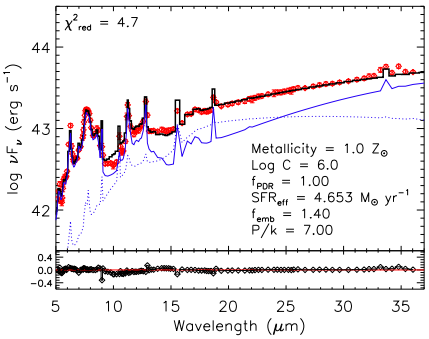

(c) NGC 1222

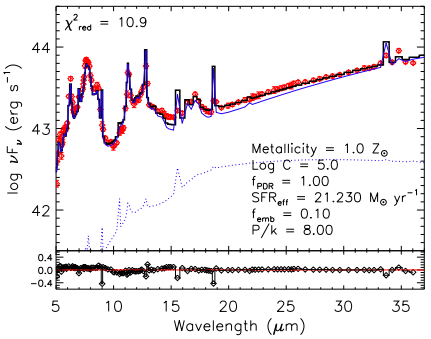

(d) NGC 4676

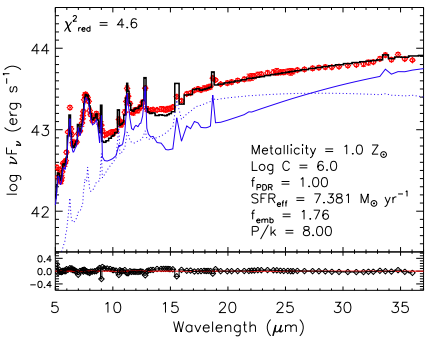

(e) NGC 7714

Figure 4.3 Best fit to the IRS spectra of our selected galaxies. Shown are the IRS data (red), best fit SED (solid black), and the different contributions of the resulting SED: the H II region (dashed blue), the PDR region (solid blue), and the embedded populations (dotted blue). The residuals are indicated in the lower panel.

the total column density of dust between us and the source. To account for the variations on the extinction we adjust the value of the dust column density, $\rho_{\rm dust}$, to reproduce the shape of the silicate absorption feature. For all galaxies, a value of $\rho_{\rm dust}$ corresponding to an optical extinction of $A_V = 1.0$ gives a good fit to the silicate feature, except for NGC 4676, for which a higher value of extinction ($A_V = 4.0$) in needed to reproduce the spectra.

Fig. 4.3 and Table 4.2 indicate that spectral differences in the MIR translate into variations in the physical conditions in starbursts of similar metallicities. In B06, the authors showed that in spite of the spectral differences, some average properties are common to all starburst galaxies, and produced an average "template" starburst spectrum. Here, we adopt a different perspective. We quantify the differences in the spatially unresolved spectra of the nuclear regions and relate them to variations in the local physical conditions of the ISM. This will allow us to investigate what physical parameters have an impact on the star formation activity of starbursts.

4.4 Discussion

Although the galaxies in our sample are all nuclear starbursts, with no significant contributions from AGNs, our results indicate that they have a broad range of physical conditions. Some of the observed differences may be related to geometrical effects unresolved by the spectrometer slit, such as orientation (mainly galaxy inclination) and size. However, it is unlikely that the pronounced differences seen in the MIR spectra of these galaxies is related to inclination effects, because very high optical depths would be necessary to affect the MIR emission in these objects. In a theoretical study by Jonsson et al. (2010), using the same physical models on which our Bayesian tool is based, the authors show that the effect of galactic inclination on the MIR SED is very small, with the only noticeable effect being a change in the 9.7 μm silicate absorption feature for very inclined galaxies. Moreover, we have also discussed in §4.3 the fact that the spectra have been scaled to match the flux of the entire region contained within the LL slit. Since the galaxies are located at different distances, this region is not always restricted to the galactic nucleus. Nevertheless, we assume that in all our objects the observed spectrum is dominated by the central starburst.

We are therefore confident that the measured differences in the spectral shapes of these objects are related to the physics of the stars and the ISM in the starbursts, with only a small dependence in geometry. In the following we interpret our findings in terms of the relation between the observed trends in the best fit parameters and the overall characteristics of the starbursts.

4.4.1 Star formation rates

In general our estimates for the SFRs agree with the literature values listed in Table 4.1. The galaxies with the most intense star formation activity in our sample are NGC 4676

and NGC 1097. Although we derive a SFR of only 5.2 $M_{\odot}$ yr^{-1} for the latter, it is worth remembering that the IRS LL slit only covers a fraction of the 1 kpc star-forming ring, and hence our estimation is only a lower limit. Assuming a uniform star formation azimuthaly distributed in the ring, the actual SFR for this starburst might be two or three times larger, and hence comparable to that of NGC 4676. These two galaxies have the highest nuclear molecular gas masses in the sample, and in both cases the nuclear molecular mass accounts for at least 20% of the total molecular gas in the host galaxies. In the remaining galaxies the molecular masses are at least one order of magnitude lower, and in the cases of NGC 1222 and NGC 4676 only upper limits have been detected.

Our estimate of the SFR is based on the integrated luminosity of the best fit SED, and as a pan-spectral diagnostic, it is more accurate than star formation diagnostics that use a single feature (e.g., the PAH emission at 7.7 μm), to estimate the total luminosity. The resulting SFRs, are correlated with the total molecular masses measured towards the nuclei. This agrees well with the star formation laws in which the SFR scales proportionally to the molecular gas content (Kennicutt 1998), and does not seem to depend much on the geometry of the nucleus. By far, IC 342 is the starburst nucleus with the lowest SFR. The amount of molecular gas in this galaxy has been estimated to be 1.0×10^7 $M_{\odot}$, lower in comparison with NGC 1097 and NGC 4676. However, it hosts a high concentration of molecular gas in the central region (Israel & Baas 2003). IC 342 is the only galaxy on the sample that is not visibly affected by interactions with nearby companions. Our result of more intense starbursts in interacting systems would support an scenario in which galactic collisions are more efficient than other mechanisms in bringing the starburst gaseous fuel together.

4.4.2 Pressure, compactness and their relation to massive clusters

We have discussed in previous chapters the relevance of the compactness parameter C in controlling the dust temperature in H II regions as a function of time, and its corresponding impact on the SED. This arises from the fact that, as the H II region evolves, the cluster mass ($M_{\rm cl}$) and the ISM external pressure P_0/k combine to set the temporal evolution of the heating flux, as parametrized by the cluster luminosity divided by the square of the H II region radius, $L_{\rm cl}/R_{\rm HII^2}$. From equation 2.1, we know that the compactness parameter is proportional to the product $\mathrm{M_{cl}^{0.6} * P_0/k^{0.4}}$. This implies that to keep compactness constant, an increase in the cluster mass must be counteracted by a decrease in ISM pressure.

Our results in Table 4.2 point to an inverse correlation between the measured compactness and pressure for our sample galaxies. Those galaxies with higher compactness are also those with lower values of P_0/k, and vice-versa. If this trend is confirmed in a larger sample of objects, it would have implications in our interpretation of the compactness. According to the definition of the compactness, to keep a high C at their low ISM thermal pressures, NGC 1222 and NGC 7714 should have a significantly higher average cluster mass as compared to NGC 1097 and NGC 4676, which also have significantly higher SFRs over the last 10 Myr. Altogether, this indicates that, even if NGC 1222 and

NGC 7714 are not forming the largest amounts of stars, they might be forming the most massive star clusters. Interestingly, as discussed in §4.2, and shown in Fig. 4.2, these two galaxies show strong nebular lines that indicate the presence of particularly massive stars.

Let us speculate in the context of the possible scenarios for the formation of massive stars. If the presence of very massive stars in the starbursts where we infer the largest average cluster masses is confirmed, this would support an scenario of competitive accretion, which requires massive stars to form in clustered environments. The reason is that competitive accretion predicts an explicit relation between the mass of a cluster and the most massive star in that cluster ($m_{\rm max}$), with $M_{\rm cl} \propto m_{\rm max}^{1.5}$ (Bonnell et al. 2004). In contrast, the core accretion model of star formation allows for massive stars to form in relative isolation. Our method can thus be combined with reliable diagnostics of the presence of very massive stars in clusters to test proposed models of massive star formation. Because of the small sample size of this pilot study, however, this is a very speculative statement, and further evidence is needed, part of which can be obtained by applying the present method to a larger sample of starbursts.

4.4.3 Molecular gas content and feedback in starbursts

NGC 1222 and NGC 7714 are also peculiar in their low molecular gas content, with only upper limits detected. IC 342 also has molecular gas mass two orders of magnitude below NGC 1097 and NGC 4676. Their low molecular content is also consistent with the lower upper limits that we have derived for their luminosity contribution from PDR regions. While this correlates well with their comparatively lower SFRs (in fact, IC 342 has the lowest SFR in the sample), the reason for the depletion of molecular gas in these starbursts is not clear. Negative feedback has been reported as a possible cause for this depletion by some authors in the particular case of IC 342 (Meier et al. 2011, Schinnerer et al. 2008). According to these authors, dense gas in IC 342 gets dispersed in the presence of an expanding H II region, and the influence of the negative feedback process can be such that it considerably diminishes the gas flow from the bar that feeds the star formation activity, thus quenching further star formation. Negative feedback from the massive clusters inferred in NGC 1222 and NGC 7714 can explain their low gas contents, not only from the expansion of H II regions, but also aided by the strong stellar winds from massive stars, and supernova activity.

However, a striking characteristic is that both NGC 1222 and NGC 7714 have the largest inferred contribution from young embedded objects, with $f_{\rm emb}$ being at least 6 times larger for these systems than for NGC 1097 and NGC 4676 (Table 4.2). We have described the interpretation for this parameter in §2.5.4. Briefly, it refers to the mass ratio of embedded to non-embedded stars that are younger than 1 Myr. If $f_{\rm emb} = 0.0$, embedded objects no longer exist in the clusters, whereas if $f_{\rm emb} = 1.0$, half of the massive stars formed over the last million year are still in a embedded state. Our results indicate that in NGC 1222 and NGC 7714, about 60% of the young (< 1 Myr) massive stars are still in an embedded phase, while only 25% of the stars of similar age are still embedded in NGC 1097, and even less in NGC 4676. For IC 342 the fraction is about 50%.

Does this apparent enhanced activity of recent massive star formation in NGC 1222 and NGC 7714 contradict their low molecular mass content? Not necessarily, for two main reasons. First, the CO surveys on which the molecular gas determination is based do not necessarily trace the very dense regions where massive stars form, which have column densities of the order of 10^{24} cm^{-2}. Second, the timescales for gas depletion in the nuclear regions are longer than the age difference between the young embedded stars and the massive main sequence stars formed over the last 10 Myr. Therefore, even if gas has been depleted over periods longer than 10 Myr, very recent events of star formation are possible (via triggering, for example) from the same primordial molecular gas cloud that formed the ionizing sources. Once again, this is an scenario that requires a more significant statistical sample of galaxies before any strong conclusions are drawn.

4.5 Summary and outlook

The MIR spectra of starbursts contain a wealth of information about recent star formation activity in galaxies, in particular in those with nuclear starbursts. In the pilot study presented in this chapter we have applied our Bayesian SED fitting tool to the MIR spectra of a small sample of galaxies whose star formation activity is dominated by nuclear starbursts. We have chosen a sample of objects with solar metallicities, in order to investigate metallicity-independent differences in their physical properties. Our Bayesian method gives robust best fit values and uncertainties to the physical parameters of these starbursts.

Overall, starbursts share some common spectral features that include PAH emission, silicate absorption at 9.7 μm, strong thermal continuum and nebular forbidden lines from atomic species, as discussed in B06. Our results show that, despite these general similarities, significant differences in the recent star formation histories of nuclear starbursts can be derived from their MIR spectra, and related to their overall properties. Our exploratory study points to a relation between the star formation rate, the gas content, and the presence of massive stars in these systems. While the SFRs in the studied starbursts correlate well with the measured mass of molecular gas, the starburst with the highest SFRs in our sample do not host the most massive derived star clusters. Instead, in our sample the most massive clusters that formed during the last 10 Myr are from starbursts with less intense SFRs, where the molecular gas is depleted, like NGC 1222 and NGC 7714. This relation requires further confirmation. Interestingly, we also find that these gas-poor systems show the largest contribution from very recent (< 1 Myr) massive star formation. Further evidence needs to be collected to investigate if feedback from the inferred massive clusters is responsible for the triggering of these new events of star formation.

We have shown in the preceding chapters the power of Bayesian SED fitting in the interpretation of spectral observations at MIR and FIR wavelengths. We have calibrated our tool using the well known nearby massive star formation regions 30 Doradus and NGC 604, and then applied it to the spectra of a small sample of starburst galaxies. We have shown the potential of the tool in the interpretation of these starburst spectra. Our results provide the first hints to interesting trends in the physical parameters of these systems

and their relation to the condition of the ambient ISM. These hints can be at the base of our understanding of starbursts, but require further confirmation. The next step is to apply the Bayesian tool to a larger sample of galaxies in order to provide statistical significance to these trends. A natural candidate sample is the Great-Observatories All-Sky LIRG Survey (Armus et al. 2009,GOALS), which includes imaging and spectroscopy data from several space-based observatories, and is unique regarding the large number of observations and their wavelength coverage. In particular, it contains *Spitzer*-IRS spectroscopy of a sample of 202 galaxies including many Luminous Infrared Galaxies (LIRGs), many of which also have available *Herschel* data. A systematic study of these objects with our method will provide some answers to the long-standing questions regarding the nature of starbursts.